Bi-level fuzzy force shaping controller of a exible wiper system

Bi-level Fuzzy Force Shaping Controller of Flexible Wiper System

Ali Zolfagharian[1,], Amin Noshadi[2], Mohd Zarhamdy Md. Zain[3],*

[1, 3] Department of System Dynamics & Control, Universiti Teknologi Malaysia, Johor, Malaysia

[2] School of Engineering and Science, Faculty of Health, Engineering and Science, Victoria University, Melbourne, Victoria, Australia

*Corresponding Author. Tel.: +989113145289, Fax: +981125232587, Email:ali.zolfagharyan@gmail.com

[1]ali.zolfagharyan@gmail.com, [2] amin.noshadi@live.vu.edu.au, [3]zarhamdy@fkm.utm.my

Abstract

In flexible manipulators the residual vibration and unwanted transient deflection are critical issues that are highly correlated the velocity operation of the system; as the velocity increases the control of such systems become more delicate and difficult. Wiper blade of automobile is among those types of flexible system that is required to be operated in quite high velocity to be efficient in high load conditions. This causes some annoying noise and deteriorated vision for occupants. The modelling and control of vibration and low frequencies noise of an automobile wiper blade is focused in this study. The flexible vibration and noise model of wiper system is estimated using artificial intelligence system identification approach. A controller approach is also developed to suppress low frequencies noise of wiper end-point while maintaining desire position accuracies of hub angle simultaneously.

Keywords: Automotive wiper, system identification, intelligence control, , multi objective optimisation

1. Introduction

Flexible structures have been broadly utilized in diverse industrial researches and designs due to their advantages like free friction loss in joints, low weight, less energy consumption and low cost. Nonetheless, control of flexible manipulators has always been a crucial issue to deal with so that convinces designer for applying them rather the traditional rigid counterparts in design. However, in some products like automobile wiper system the flexibility is an inherent characteristic that cannot be alternated. Wiper system is an indispensible part of an automobile with flexible nature. Flexibility feature of wiper blade structure is made it a critical apparatus is spite of its simple operational mechanism. A desirable wiper system is characterized by a homogeneous disposal of the water, without noise generation and by limiting as much as possible the phenomenon of wear (loss of wiping or noise presence). An experimental method verified with a finite element analysis is carried out for past processing system identification and control of wiper system [1]. Low frequency noise known as chatter noise were identified in wiper system during operation and is subjected to be suppressed while does not violate other oscillatory attributions of wiper system in time domain. This noise causes annoying sound to automobile occupant within the wiper operation especially in the heavy rain and snow.

The vibration control of chaotic motion in a two blades wiper system was investigated by Wang Chau [2]. Friction effects between windscreen and wiper blade and its variation in accordance to temperature as well as velocity of wiper motor were investigated [3], [4]. Inverse dynamics control in cooperation with input shaping was developed to achieve minimum vibration within bounded speed of drive [5]. Singla proposed a hybrid control method for a flexible inverted pendulum on a moving cart that deals with the vibration of system with minimum actuator effort [6]. Yanyan [7] proposed a control approach by sensing the rain extent on windscreen using infrared rain sensor that commands the motor velocity proportionally. Several methods like dither signal, extended time-delay feedback control and the optimized command shaper control methods were applied for controlling the chaotic motion of wiper blade [2], [8].

Flexible dynamic of a wiper system requires a reliable system identification method to model transfer function of wiper system for helping designer in developing more accurate controller. Modeling of wiper system as a flexible manipulator with several modes needs a trustworthy system identification method featuring capability at fast varying dynamics and non-minimum phase systems modeling [9], [10]. A Nonlinear auto regressive exogenous (NARX) [11] in cascade with Elman neural network (ENN) [12] is utilized for the purpose of system identification of nonlinear wiper system.

Input shaping (IS) method as an effective Feed-forward controller is chosen for noise reduction and improving other dynamic characteristic of flexible wiper blade [13]. Input shaping approach is highly depends on system natural frequencies and damping ratios. Employing this method signifies the necessity of precise system identification. Comparison studies of responses of flexible manipulator by various feed-forward controller techniques were studied by Azad et al [14]. The results proved the superiority of input shaping technique in terms of vibration reduction at first three modes, settling time and overshot rather to Gaussian shaped and low-pass filtered input torque. Also, though Gaussian method had better performance in terms of attenuation of power spectral density (PSD) compare to low-filtered input torque; it performed worse based on time responses criteria.

In order to handle great performance of control system within uncertain circumstances, traditional controllers such proportional, integrative, derivative (PID) controllers are not the best choice due to constraints imposed on gains regulation. Fuzzy logic controller (FLC) has advantage of control a system by means of expert knowledge and regardless of actual dynamic of plant [15]. Some applications of FLC in flexible link control, system identification and parallel manipulator control problems can be found in literature. [16], [17]. Also, some efforts were done for cooperating FLC with evolutionary and swarm approaches [16], [18].

In multi objective control problem it is necessary to estimate a number of parameters or gains for the control scheme that in turn introduces more complexity to the scheme. To tackle this, MOGA is utilized in control loop in order to attain a trade off solution. Multi-objective Genetic Algorithm (MOGA) using fitness sharing technique is adopted in this study due to its versatile character of dealing with various conflict objectives and their constraints. MOGA based on fitness sharing have been successfully applied in other control engineering problems of flexible manipulators [19], [20].

The lack of exotic techniques that target the vibration and noise reduction of wiper blade in both time and frequency domains simultaneously persuaded this research. A reliable nonlinear system identification namely (NARXENN) was adopted in first stage of this survey to model the flexible dynamics of wiper blade with acquired experimental data. A zero-vibration-derivative-derivative (ZVDD) IS controller was designed based on the dynamics properties of wiper system extracted from system identification and applied on the path of reference input. Then, closed loop control integrating FLC and AFC was developed to add robust trait to controller for possible uncertainty that occurs during operation of wiper. In order to deal with complexity of controlling the multi conflict objectives in both time and frequency domains MOGA is utilized to regulate the corresponding parameters of proposed controller. Detail of the proposed controller is illustrated in **Fig. 1.**

Fig.1----------

This paper presents data acquisition and experimental set up in section 2. Also, mathematical and conceptual explanation of system identification and control strategies are briefly described. Effectiveness and results of applying the proposed controller are discussed in section 3. Paper concludes in section 4.

2. Methodology

2.1. Data Acquisition

First, the data acquisition stage is carried out on-line for recording the wiper system signals. Then, the data analyses run off-line and handle the recorded data to develop an efficient controller standing by experimental tests.

A uni-blade type wiper which is typically found in the Proton Iswara driven by its corresponding DC Wiper Motor in hub, measuring devices, interface card and digital processor are in hand for experiment. The wiper blade can be considered as a pinned-free flexible arm that moves freely in the horizontal plane of windscreen while the effect of axial force is negligible. A pipe hose with running water is facilitated on the top of windscreen that simulates a rainy or wet condition for operating wiper at speed of Bang-Bang input. The measurement sensors including a Kistler Type 8794A500 tri-

axial accelerometer mounted at the endpoint of the wiper blade using beeswax for measurement of endpoint acceleration as well as a shaft encoder placed at the hub of wiper for measurement of hub angle. Recording the input signals is carried out at digital sampling rate of *1* kHz.. In the experiment, a 16 input channels PAK MK II Muller BBM signal analyzer were used.

The simulation of the flexible manipulator is conducted with the two analogue outputs namely hub angle and end-point acceleration. Low-pass (LP) filters each with cut-off frequency of 80 Hz is used to band limit the system response to the first resonance mode for each output. Furthermore, to decouple the flexible motion control loop from the rigid body dynamics a high-pass filter for each output with a cut-off frequency of 5 Hz is used. The system damping ratio is negligible and payload is measured as 7.4 N/m. A motor drive amplifier (current amplifier) delivers a current proportional to the input voltage for actuating a bi-directional motor. A linear drive amplifier LA5600 can be employed as motor driver too. The shaft encoder placed on hub of wiper send the analogue information of the hub angle of the wiper to process unit of controller after being converted to digital values. An interface circuit PCL 812PG is needed to interface the wiper system with a host PC and carrying out data acquisition and control between the processor, the actuator and sensors with 25 μs for A/D conversion and a settling time of 20 μs for D/A conversion. A schematic diagram of proposed controller interfaces used in this work is shown in **Fig. 2**.

Fig.2----------

2.2. Nonlinear Auto Regressive Exogenous Elman Neural Network (NARXENN)

The NARX model structure is defined by

$$y(k) = F\left(y(k-1), \dots, y\left(k-n_y\right), u(k-1), \dots, u(k-n_u)\right) + \varepsilon(k), \quad (1)$$

in which the effect of noise is assumed additive at output of the model. *F(.)* is a nonlinear function, y_k ,u_k and ε_k are output, input, and noise respectively where n_y, n_u and are maximum lags on observations and exogenous inputs [11]. In order to identify the NARX model; the corresponding *F(.)* function should be approximated first; so that in this study the nonlinear function *F(.)* is estimated by ENN.

In the structure of an ENN there is an additional undertake layer called context layer besides the three conventional namely input, hidden and output layers that making the identification of dynamic characteristics [12]. Suppose an ENN such is shown in **Fig. 3** in which the vectors of input, middle and output layers' nodes are labeled with *u*, *x* and *y* respectively. Also, W_1 , W_2 and W_3 represent the respective connection weights of input, middle and output layers. The nodes of input layer play the role of signal transmission while nonlinear functions of *M(.)* and *O(.)* are introduced as transfer functions of middle and output layers which in this study the tansigmoid function is used. Furthermore, the previous moment output values of hidden layer were stored in memory and return to the input, so it can be considered a step delay operator. The mathematical modeling of Elman Neural Network can be expressed as the following equations:

$$X(k) = M\left(W_2.u(k) + W_1.u(k-1)\right) \quad (2)$$

$$y(k) = O\big(W_3.x(k)\big) \tag{3}$$

A back propagation (BP) algorithm as it broadly used and discussed in literature was adopted for training process of neural network. BP uses the error sum of squares function between output of network and target values [21]:

$$E(W) = \sum_{n=1}^{k}[y_n(W) - T_n(W)]^2 \ , n = 1,2,3,\dots,k \tag{4}$$

where $T_n(W)$ is the target vector of output.

Schematic model of proposed system identification named nonlinear auto regressive Elman neural network (NARXENN) is illustrated in **Fig. 3**.

Fig. 3----------

2.3. Non-collocated control

The AFC technique verified to be quite effective in robust accuracy positioning tasks in spite of possessing trouble-free mathematical algorithm [22].

Investigations on applying AFC as non-collocated control technique showed that by using this method, the system subjected to environment uncertainties and disturbances remains stable and robust. The successful operation of AFC method as a disturbance rejecter scheme compared to the traditional control methods such as the PID controller is proven in the literature [17], [21].

Other advantages of application of AFC as a disturbance rejection in this study are because of its low computational burden and few input information in a real time system. As it is shown in **Fig. 4** AFC requires only the acceleration information of wiper tip.

In the rotational bodies, Newton's second law expresses that, the sum of all torques applied to the system is equal to the multiplication of the mass moment of (I) to the angular acceleration (α) of the system, i.e. from

Considering well-known and functional second Newton law of motion of rotational bodies as:

$$\sum \boldsymbol{\tau} = I\alpha \tag{5}$$

Where $\boldsymbol{\tau}$ is the applied torque of wiper motor and I and α are the mass moment of inertia and the angular acceleration of the wiper blade respectively.

An external disturbance $\boldsymbol{\tau}_{\mathrm{d}}$ is included in (1):

$$\boldsymbol{\tau} + \boldsymbol{\tau}_{\mathrm{d}} = I(\theta)\alpha \tag{6}$$

The main point of AFC is where disturbances have to be estimated somehow as:

$$\boldsymbol{\tau}_{\mathrm{d}}^{*} = \boldsymbol{\tau} - \boldsymbol{EI}\alpha \tag{7}$$

where $\boldsymbol{EI}$ is the estimated inertia matrix that can be obtained by crude approximation or other intelligent methods such as iterative learning, fuzzy logic and so on. MOGA has been used in this

paper to estimate the most appropriate value for $\boldsymbol{EI}$ to achieve a desirable trade off among all objectives even in presence of external disturbance. $\boldsymbol{\tau}$, is the measured applied control torque that can be estimated by a current sensor or directly by a force or torque sensor and the measured angular acceleration, i.e., $\ddot{\theta}$ can be obtained by an accelerometer. From (7) it is clear that if the total applied torque to the system and angular acceleration of each actuated joint are accurately obtained using measuring instruments and the estimated inertial parameters are needed in AFC loop for disturbance rejection are appropriately approximated, without having to acquire the knowledge about actual magnitude of the disturbance, the total torque disturbances can be rejected using AFC loop. A schematic diagram of developed AFC method as part of the proposed controller was depicted in the **Fig. 4**.

Fig. 4----------

2.4. Collocated controller

A fuzzy controller with two inputs named, the track error and rate of track error of the wiper hub displacement and one output which is in the path of a scale factor is adopted in collocated control part (**Fig. 5**). The inputs and output of the fuzzy controller are normalized within range of $[-1,1]$ while the appropriate location of membership functions' inputs as well as scale factor parameters have been tuned by MOGA for normalization purposes based on the following conditions:

$$TE = \max(-1, \min(1, S_{TE})) \tag{8}$$

$$\delta TE = \max(-1, \min(1, S_{\delta TE})), \tag{9}$$

where TE and δTE represent the track error and rate of tack error for hub displacement of wiper respectively. S_{TE} and $S_{\delta TE}$ are the best position of membership functions of TE and δTE which are aimed to be adjusted by MOGA. Similarly, the FLC output is denormalized using $U = S_u.\hat{u}$. Membership functions of the inputs and output of fuzzy logic controller are shown in **Fig. 6**.

Fig. 5----------

Fig. 6----------

The different values of S_{TE} for track error and $S_{\delta TE}$ for rate of tack error of controller lead to various shape of triangles. Since, the FL output is manipulated by S_u factor that is fine tuned by MOGA, the positions of output membership function ($\pm d$) are supposed to be constant as d=$\pm$0.5.

For the two inputs as well as output of the FLC five triangles membership function were chosen for each; and a complete rule matrix of size 5×5 is defined in **Table 1**.

Table.1----------

The *n*th command of the rule base for the FLC, with track error and rate of track error as fuzzy inputs and $\hat{u}$ as fuzzy output, is given by:

C_n: If TE is NB and δTE is ZE then the $\hat{u}$ is PB

A two level fuzzy tuning methods whose normalized output parameter (S_u) as well as nonlinear tuning parameters (S_{TE}) and ($S_{\delta TE}$) are adjusted by means of MOGA is developed. The superiority of the proposed controller similar works is tuning nonlinear parameters of FL input membership that increase the robustness and performance of the controller without exceeding the maximum permitted value of S_u scale factor.

2.5. Open-loop input shaping control

Input shaping's mathematic derivation for two-impulse sequence can be obtained as following. Transfer function of a second order system whose *n*th natural frequency and damping ratio are ω_n and ξ respectively can be stated as follow:

$$T(s) = \frac{\omega_n^2}{s^2+2\xi\omega_n s+\omega_n^2} \tag{10}$$

The residual vibration resulted from a series of impulses utilized in the system can be derived from second order system transfer fuction as [13]:

$$V(\omega,\xi) = e^{-\xi\omega_n}\sqrt{\left(\sum_{i=1}^{N} P_i\,(\omega,\xi)\right)^2 + \left(\sum_{i=1}^{N} Q_i(\omega,\xi)\right)^2} \tag{11}$$

$$\begin{aligned} P_i &= A_i e^{-\xi\omega t_i}\cos(\omega_n\sqrt{1-\xi^2}t_i) \\ Q_i &= A_i e^{-\xi\omega t_i}\sin(\,\omega_n\sqrt{1-\xi^2}t_i\,) \end{aligned} \tag{12}$$

where A_i is amplitude, t_i represents the time of the impulses and *n* is the number of impulses in the impulse sequence.

As the number of impulse shaper increases the controller becomes more robust due to the increase in rise time. So, the number of impulse shapers is a compromise which is determined based on design specifications. A ZVDD input shaper that is comprised of four-impulse shaper is employed in this study. The time and location of four impulses ZVDD is listed in **Table 2**.

Table.2----------

In the case of this study first natural frequency of wiper system is inferred from results of data acquisition and system identification as approximately 11 Hz. Also, damping ratio of wiper system is estimated using finite element analysis as 0.16 [23].

2.6. MOGA

Fitness sharing based MOGA is utilized to give confidence in the search toward the true Pareto optimal set while maintaining diversity in the population [24]. The basic idea of fitness sharing is that all the individuals within the same region (called a niche) share their fitness. In fitness sharing method first a niche count is obtained from the Euclidean distance between every solution pair and then the

fitness of each solution is assigned from the best individual to the worst according to some function, in the form of fitness function, such as linear or exponential, possibly other types. The greater fitness is understood here as the number of individuals decrease in the same rank. The stochastic universal sampling method is used to select the best individuals [25]. However, mating restrictions are employed in order to protect lethal [26]. In a multi objective Pareto based optimization problem it shall be assumed that the true Pareto front is unknown; therefore the only means of evaluation available is to compare the MOGA solutions against each other. Hypervolume indicator is adopted in this study for performance assessment of MOGA [27].

3. Results and Discussions

3.1. Establish the cost functions

Three objectives of wiper system's dynamic characteristics are defined to be considered in this study. Integral of absolute end-point acceleration (IAEA), maximum overshot of hub displacement and rise time of hub displacement response; are objectives that are aimed to be minimized and defined as:

- Integral absolute value of end-point acceleration (IAEA):

$$IAEA = \int_0^T |y_{EA}(t)|\, dt, \tag{13}$$

where $|y_{EA}(t)|$ denotes the end-point acceleration of wiper blade. IAEA integrates the area of acceleration response of wiper blade respect to time. IAEA is an index of noise level of wiper blade.

- Rise time: The time required for system hub displacement response to rise from 5% to 95% of the final steady state value of the desired response.
- Maximum overshoot: The maximum peak value of the hub displacement response curve measured from the desired response of the system.

In the engineering pursuit, designers are frequently come across with trade-off problems. In the design of proposed Bi-level fuzzy force shaping controller such trade-off is emerged in relationship between rise time and vibration amplitude. Typically, in flexible manipulator and structure dynamics control often the low levels of residual vibration cannot be obtained with a command that produces the fastest rise time [28], [29]. In most cases, to achieve the low levels of vibration and highest robustness, the rise time must be increased which in not desirable. IAEA and maximum overshoot are objectives in accord; while the rise time index of wiper lip is in obvious conflict with two aforementioned objectives.

3.2. System Identification

For the modeling process, input-output data were collected for a wiper system. Then, performing the one value at the moment the best maximum lag of the data in NARX model was found as $n_x = n_y = 7$. Subsequently, ENN with two hidden layers, each with 10 tansigmoid neurons and two linear output layers was trained. The process is adjusted until the prediction output satisfied a model validation test and model mean squared errors (MSE) level reached to 0.000048. The fitting accuracy

of predicted system for one step ahead (OSA) prediction of the corresponding end-point acceleration and hub-angle responses of the actual system compared to NARXENN are shown in **Fig. 7.**

The illustrated results of actual and predicted PSD and Yule Walker power/frequency of end-point acceleration in frequency domain in **Fig. 8** prove that, there is an acceptable comparison between system identification results and actual results in frequency domain as well.

Fig.7----------

Fig. 8----------

3.3. Input Shaping Controller for single objective

First, ISC is designed based extracted natural frequency and damping ratio of wiper model is applied to system. **Figs. 9** and **10** show IS controller is capable of reducing the vibration and noise at the end-point of the manipulator in an open-loop control without intervention of any external disturbance.

Nonetheless, further study revealed the deficiency of IS controller in vibration and noise elimination of wiper blade in presence of external disturbance and uncertainty (**Fig. 14)**. Hence, an essence of an effective controller for reduction of chatter noise level of wiper blade simultaneously with accurate trajectory tracking of wiper hub angle was demanded. In order to achieve such controller it is required to add closed-loop controller for flexural motion control of the system. An extended control structure for control of a flexible wiper blade is devised. In the proposed controller two different loops of AFC and FLC are accumulated to send most accurate command to input torque to reject any unknown external disturbance. The control scheme has been devised within a simulation environment and is standing by an experimental rig.

Fig.9----------

Fig.10----------

To validate the effectiveness of the proposed controller in presence of external disturbance a harmonic disturbance (τ_d) is imposed to the wiper over the time in following investigation:

$$\tau_d = 2\cos(t) \tag{10}$$

3.4. Bi-level Fuzzy Force Shaping Control Regulated for Multi Objectives

Hypervolume indicator assesses the convergence of algorithm toward Pareto front as well as preserving the distribution of Pareto front throughout objectives space. In other words, this metric explores the extent of the objective space covered by a set of solutions which is restricted by setting a suitable reference point. In case of minimization problem, like the case of current paper the reference point is set in such a way that exceeds the constraint of each objective. Therefore, once this metric is applied to compare the performance of an algorithm in successive iterations; as the number of non-dominated solutions and their distribution throughout the objective space increases the Hypervolume indicator's value represents the greater value

MOGA initialized with a random population consisting of 50 individuals and maximum generation of 100 as termination criterion. The population is represented by binary strings each of 30 bits, called chromosomes. Each chromosome consists of five separate strings constituting rest three terms are specified to FL membership positions and the rest two are specified proportional and integrative sale factors of BFFS controller. Using educated guess a reasonable range of these parameters that ensure stability of system is defined. The crossover rate and mutation rate for this optimization process were set at 90% and 0.01%, respectively. Moreover, Epanechnikov fitness sharing genetic technique was used to ensure that the best solution of each generation is selected for the next generation so that the next generation's best will never degenerate and hence guarantee convergence of the GA optimization process.

Hypervolume indicator of MOGA for adjusting controller parameters is sown in **Fig. 11**. It can be clearly seen that the overall number of Pareto front members found in each generation and their diversity throughout the objective space are increased as the number of generations goes on so that the maximum value of Hypervolume is obtained at last generation.

Fig.11----------

Fig. 12 illustrates the explicit conflict of maximum overshot and IAEA for Pareto optimal sets of wiper blade objectives. This miscorrelation makes the decision tough for designer to choose the best trade-off. However, the non-dominated Pareto set depicted in **Fig. 12** proves that IAEA and maximum overshot are highly non-competing, and it is important for the decision maker, as it conceptually reduces the complexity of the problem.

Fig.12----------

Adjustable parameters of BFFS controller and their corresponding objectives measures are inserted in **Table 3**. In **Table 3** the most significant non-dominated samples of Pareto optimal sets swinging between the robustness performances and rise time improvement of wiper blade is shown. It can be deduced that the smallest rise time of system is obtained in Trade 2 with unfavorable IAEA and maximum overshot. Further, the least amounts of vibration objectives are achieved in sol. 6 at the expense of longest rise time. However, in case of current design, the Trade 3 is deemed to be preferred to others that lead to the most reasonable values of IAEA, maximum overshot and rise time of wiper blade. Glimpsing at other tradeoffs in **Table 3** reveals that though Trade 5 has greater vibration reduction and wiper hub trajectory tracking rather Trade. 3 but this is achieved at the expense of longer system delay or rise time. Also, diverse compromised of objectives can be seen in other solutions, shown in the table so that each of them can be obtained by adjusting the location of membership functions as well as corresponding scale factors of AFC.

Table 3----------

An instances trade off of Pareto front sets for IAEA, rise time and maximum overshot of wiper blade is shown in **Fig. 13.** The x-axis shows the design objectives and the y-axis signifies normalized values of each objective. The conflict interests of objectives are deduced from crossing lines between adjacent objectives while parallel lines are evident of mutual interests between the objectives.

Fig.13----------

Bearing in mind the most important mission of proposed controller to achieve most appropriate vibration and noise reduction of wiper blade in frequency domain as well as maintaining the minimum rise time of system simultaneously convince the designer to vote on behalf of Trade. 3 with the estimated values of IAEA, maximum overshot and rise time of wiper blade *178*, *27* and *0.26 s* respectively.

The evidence of robustness of developed controller can be deduced from **Fig. 14**, which shows the response of wiper lip acceleration and tracking the desired Bang-Bang input task. **Fig. 14a** proves the significant dampening of end-point acceleration using the proposed controller rather the IS alone in the presence of disturbance. In **Fig. 14b** the high distortion of open loop wiper lip in tracking the desired trajectory in present of uncertainty is obvious while the least fluctuation in minimum rise time has been attained using the proposed controller. Furthermore, the deficiency of IS controller in comparison to the developed controller with applying external disturbance can readily be seen in terms of end-point acceleration, rise time and maximum overshot.

Moreover, the effectiveness of proposed controller for suppressing chatter noise of wiper system is shown in **Fig. 15**. It was found that the PSD and Yule-Walker amplitude of the wiper end-point significantly reduced with applying BFFS controller compared to Bang-Bang input and even solitary IS controller with presenting the disturbance. Performance measurements of various controllers in normalized index are illustrated in **Fig. 16.** It is evident that, substantial attenuation is achieved with applying BFFS compared to open-loop and IS controller in presence of disturbance.

Fig.14----------

Fig.15----------

Fig.16----------

4. Conclusion

Control of flexible wiper system is split into two tasks; one is to track the Bang-Bang input of hub angle as open-loop control and two is to reduce chatter noise and unwanted vibration of wiper blade applying collocated and non-collocated closed-loop controller. IS controller is designed based on the priory knowledge of wiper dynamics system from NARXENN system identification. IS controller was implemented outside the feedback loop and was capable to reduce vibration and noise of wiper system in a free disturbance circumstance. Insensible and deteriorated response of IS controller to uncertainties persuaded the study to devise a feedback controller. Hence, two level closed loop controller which consists of collocated FLC and non-collocated AFC were extended. MOGA applied to achieve an optimum trajectory planning of the wiper hub at reasonable rise time. It was shown that increasing the robustness to parameter uncertainties does not lengthen the duration of the transient time characteristics.

References

[1] Awang I.M., AbuBakar A.R., Ghani B.A., Rahman R.A., Zain M.Z.M., Complex eigenvalue analysis of windscreen wiper chatter noise and its suppression by structural modifications, Int. J. Vehic. Struc. Syst. 1(1-3), (2009) 24-29.

[2] Wang Z., Chau K.T., Control of chaotic vibration in automotive wiper systems, Chaos Soliton. Fract., 39, (2009) 168–181.

[3] Koenen A., Sanon A., Tribological and vibroacoustic behavior of a contact between rubber and glass (application to wiper blade), Tribol. Int. 40 (2007) 1484–1491.

[4] Bodai G., Goda T. J., Sliding friction of wiper blade: Measurement, FE modeling and mixed friction simulation, Tribology International 70 (2014) 63–74.

[5] Sahinkaya M N, Input shaping for vibration-free positioning of exible Systems, Proc Instn Mech Engrs Vol 215 Part I, IMechE 2001, 467-481.

[6] Singla Ashish, Vibration Suppression of a Cart-Flexible Pole System Using a Hybrid Controller, Proceedings of the 1st International and 16th National Conference on Machines and Mechanisms (iNaCoMM2013), IIT Roorkee, India, Dec 18-20, 2013.

[7] Yanyan W., Jiana W., Zhifu Z., Design of Intelligent infrared Windscreen Wiper based on MCU, Procedia Engineering 15 (2011) 2484 – 2488.

[8] Zolfagharian A., Zain M.Z. Md., Abu Bakar A.R., As'arry A., Suppressing Chatter Noise in Windscreen Wiper Operation Using a Robust Hybrid Controller, Int. Rev. Mech. Egr. (I.RE.M.E.), 6(3) (2012) 630-635.

[9] Shaheed M. H., Tokhi M.O., Dynamic modelling of a single-link of a flexible manipulator: parametric and non-parametric approaches, J. Robotica, 20 (2002) 93-109.

[10] Warwick J. K., Kang Y. H., Mitchell R. J., Genetic least squares for system identification, Soft Computing, 3 (1999) 200-205.

[11] Chen S., Billings S.A. Representations of non-linear systems: the NARMAX model, Int. J. Control 49 (1989) 1013-1032.

[12] Elman J., Finding structure in time, J. Cognitive Sci., 14 (1990) 179-211.

[13] Singer N.C. and Seering W.P., "Reshaping command inputs to reduce system vibration," Trans. of ASME: J. of Dynamic Systems, Measurement and Control, vol. 112 no. 1, pp. 76–82, 1990.

[14] Azad A.K.M., Shaheed M.H., Mohamed Z., Tokhi M.O. and Poerwanto H., "Open-loop control of flexible manipulators using command-generation techniques," In M.O. Tokhi and A.K.M. Azad (Ed.) "Flexible robot manipulators modelling, simulation and control," London, United Kingdom: The Institution of Engineering and Technology, 2008, pp. 207-233.

[15] Zadeh L.A., Outline of a new approach to the analysis of complex systems and decision processes, IEEE Trans. Syst. Man Cyb. 1 (1973) 28–44.

[16] Alam M.S., Tokhi M.O., Hybrid fuzzy logic control with genetic optimisation for a single-link flexible manipulator, Engineering Application of Artifitial Intelligence 21 (2008) 858–873.

[17] Noshadi A., Mailah M., Zolfagharian A., Intelligent active force control of a 3-RRR parallel manipulator incorporating fuzzy resolved acceleration control, Appl. Math. Modell., 36(6), (2011) 2370-2383.

[18] Chatterjee A., Pulasinghe K., Watanabe K., Izumi K., A Particle swarm optimized fuzzy–neural network for voice-controlled robot systems, IEEE Trans. Ind. Electron., 52(6) (2005) 1478-1489.

[19] Silva V.V.R., Fleming P.J., Sugimoto J., Yokoyama R., Multiobjective optimization using variable complexity modelling for control system design, Appl. Soft Comput. 8 (2008) 392–401.

[20] Toha S.F, Tokhi M.O., A hybrid control scheme for a twin rotor system with multi objective Genetic Algorithm, Proceeding of the 12th International Conference on Computer Modelling and Simulation, IEEE, 2010, pp 110-115.

[21] Srinivasan B., Prasad U.R., Rao N.J., Backpropagation through adjoins for the identification of non-linear dynamic systems using recurrent neural models, IEEE Trans. Neural Networ., 5(2) (1994) 213–228.

[22] Hewit J.R., and Burdess J.S., Fast Dynamic Decoupled Control for Robotics Using Active Force Control, Mechanism and Machine Theory, Vol. 16, No. 5, (1981) 535-542 .

[23] Zolfagharian A., Noshadi A., Khosravani M.R., Zain M.Z. Md, Unwanted noise and vibration control using finite element analysis and artificial intelligence, Appl. Math. Modell. (2013), http://dx.doi.org/10.1016/j.apm.2013.10.039.

[24] Fonseca C.M., Fleming P.J., An overview of evolutionary algorithms in multiobjective optimization, Evol. Comput., 3(1) (1995) 1-16.

[25] Goldberg D.E., Richardson J., Genetic algorithms with sharing for multimodal function optimization, In J. Grefenstette, (Ed.), Proceedings of the Second International Conference on Genetic Algorithms, Hillsdale, NJ: Lawrence Erlbaum Associates, 1987, pp. 41-49.

[26] Deb K., Multi-objective optimization using evolutionary algorithms, Chichester: Wiley, New York, 2001.

[27] Zitzler E., Thiele L., Multiobjective evolutionary algorithms: a comparative case study and the strength Pareto approach. IEEE Trans. Evol. Comput., 3(4) (1999) 257–71.

[28] Tokhi M.O., Zain M.Z.M., Hybrid learning control schemes with acceleration feedback of a flexible manipulator system, Proceedings of the Institution of Mechanical Engineers, Part I: Journal of Systems and Control Engineering 220 (4) (2006) 257–267.

[29] Zain M.Z. Md., Tokhi M.O., Mohamed Z., Hybrid learning control schemes with input shaping of a flexible manipulator system, Mechatronics 16 (2006) 209–219.

Lists of Tables Captions

Table 1. FLC rule base with track error and rate of track error

Track error (TE)	Rate of track error (δTE)		
	N	Z	P
N	P	P	Z
Z	P	Z	N
P	Z	N	N

Table 2. Magnitude and time location of four-impulse IS (ZVDD)

$\boldsymbol{i}$	A_i	t_i
1	$\frac{1}{(G+1)^3}$	0
2	$\frac{3G}{(G+1)^3}$	$\frac{Td}{2}$
3	$\frac{3G^2}{(G+1)^3}$	Td
4	$\frac{G^3}{(G+1)^3}$	$\frac{3Td}{2}$

Table 3. Controller parameters and objective values

Trade No.	Objectives			Controller parameters			
	$IAEA$ m/s^2	Rise time (s)	Max. overshot (%)	S_{TE}	$S_{\delta TE}$	S_u	EI
1	978	0.11	84	0.517	0.127	0.402	2.940
2	553	0.19	69	0.623	0.594	0.163	3.184
3	178	0.26	27	0.657	0.737	0.127	1.146
4	522	0.20	42	0.118	0.245	0.644	5.637
5	127	0.35	8	0.241	0.172	0.387	2.286

Lists of Figures Captions

Figure No.	Captions
Figure 1	Bi-level active shaper fuzzy force Controller using MOGA
Figure 2	Schematic diagram of proposed controller interfaces
Figure 3	NARXENN system identification of wiper system
Figure 4	Non-collocated AFC
Figure 5	Collocated FLC
Figure 6	Membership functions illustration of FLC: **(a)** Track error input; **(b)** rate of track error input; **(c)** controller output
Figure 7	Time domain modeling of wiper lip response: **(a)** End-point acceleration of wiper lip; **(b)** Hub displacement
Figure 8	Frequency domain modeling of wiper lip response: **(a)** PSD of end-point acceleration; **(b)** Yule-Walker spectral density of end-point acceleration
Figure 9	Time domain response of wiper lip without disturbance: **(a)** End-point acceleration of wiper lip; **(b)** hub displacemen
Figure 10	Frequency domain response of wiper lip without disturbance: **(a)** PSD of end-point acceleration; **(b)** Yule-Walker spectral density of end-point acceleration
Figure 11	Hypervolume indicator of wiper system objective space using MOGA
Figure 12	Optimal Pareto sets illustrations of pair objectives: **(a)** conflict interests; **(b)** mutual interests
Figure 13	Trades off samples among three objectives' Pareto set
Figure 14	Time domain response of wiper lip in presence of disturbance: **(a)** End-point acceleration of wiper lip; **(b)** hub displacemen
Figure 15	Frequency domain response of wiper lip in presence of disturbance: **(a)** PSD of end-point acceleration; **(b)** Yule-Walker spectral density of end-point acceleration
Figure 16	Performance measurements of controllers

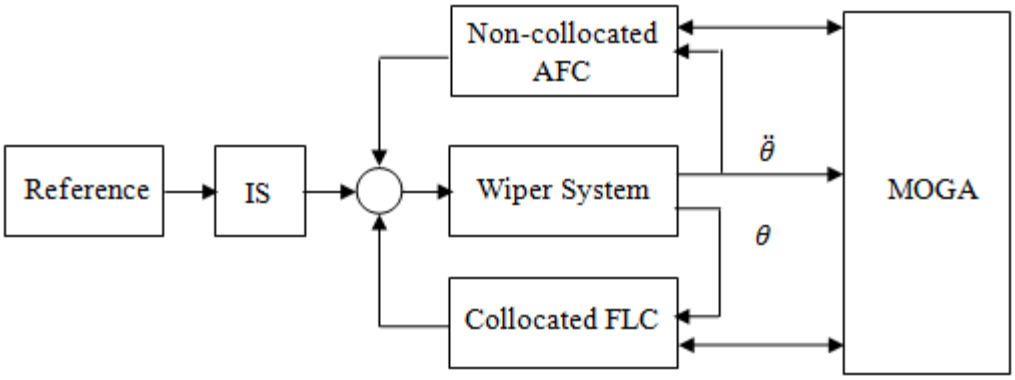

Fig.1. Bi-level active shaper fuzzy force Controller using MOGA

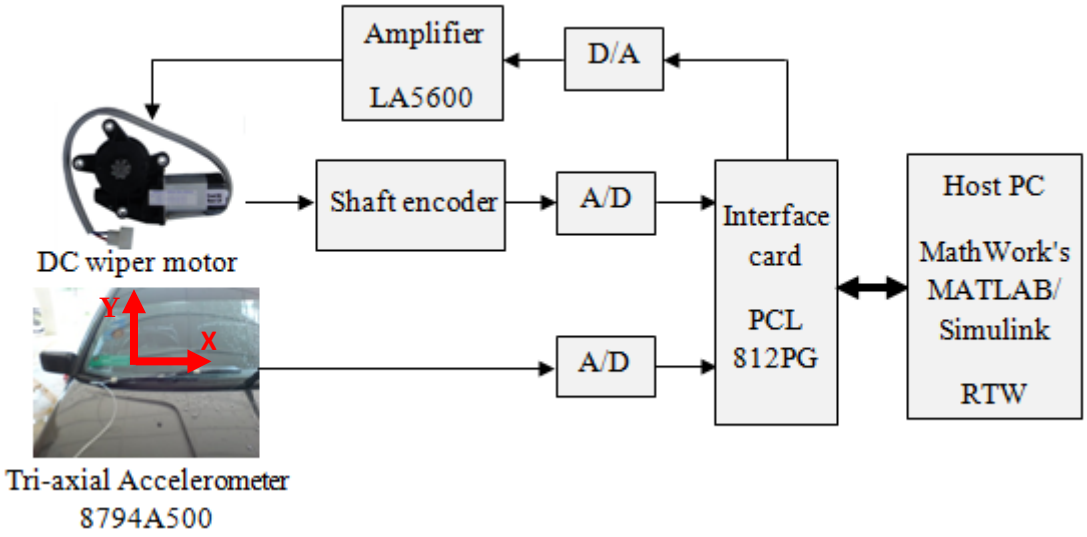

Fig. 2. Schematic diagram of proposed controller interfaces.

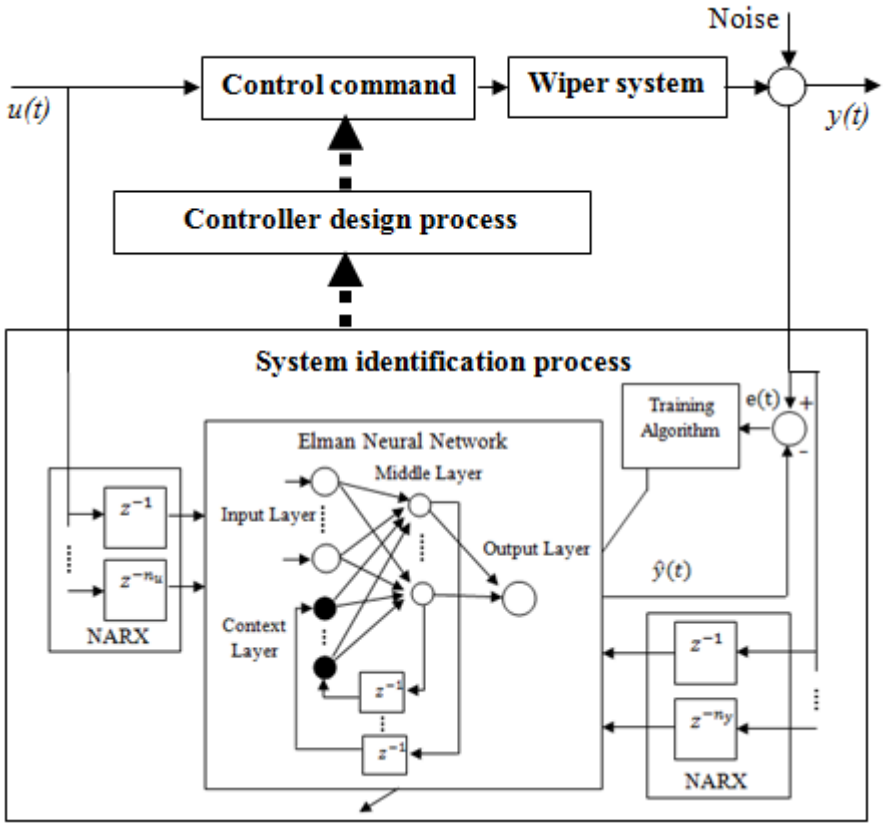

Fig. 3. NARXENN system identification of wiper system

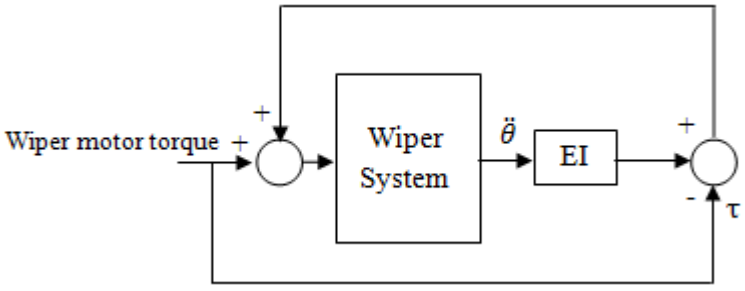

Fig.4. Non-collocated AFC

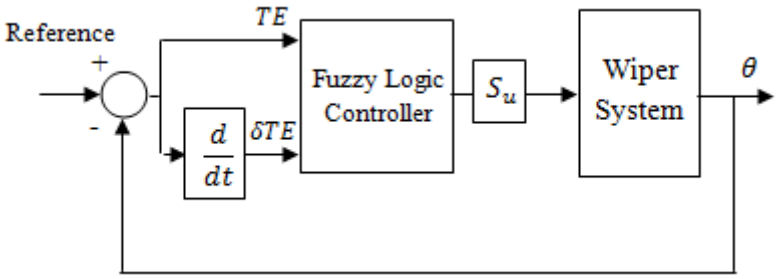

Fig.5. Collocated FLC

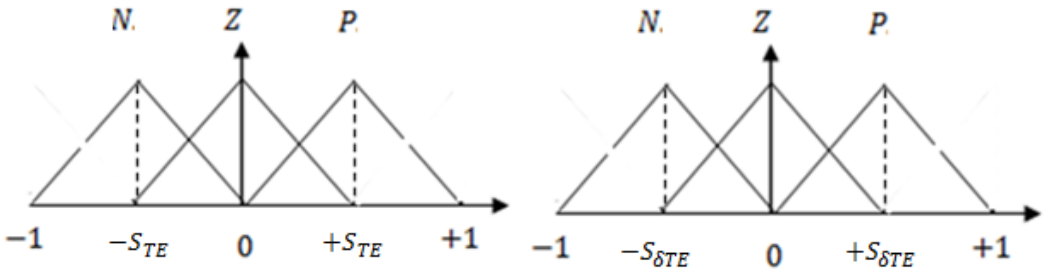

(a) **(b)**

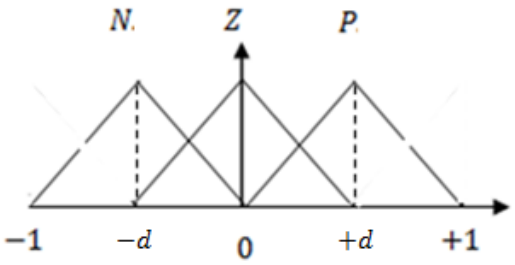

(c)

Fig. 6. Membership functions illustration of FLC: **(a)** Track error input; **(b)** rate of track error input; **(c)** controller output

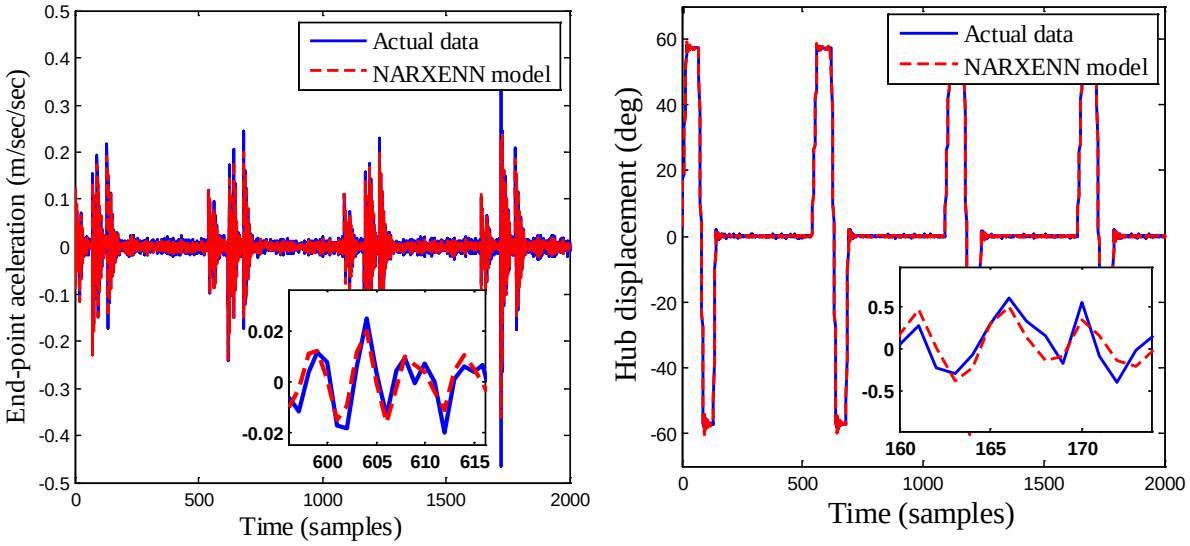

(a) (b)

Fig. 7. Time domain modeling of wiper lip response: **(a)** End-point acceleration of wiper lip; **(b)** Hub displacement

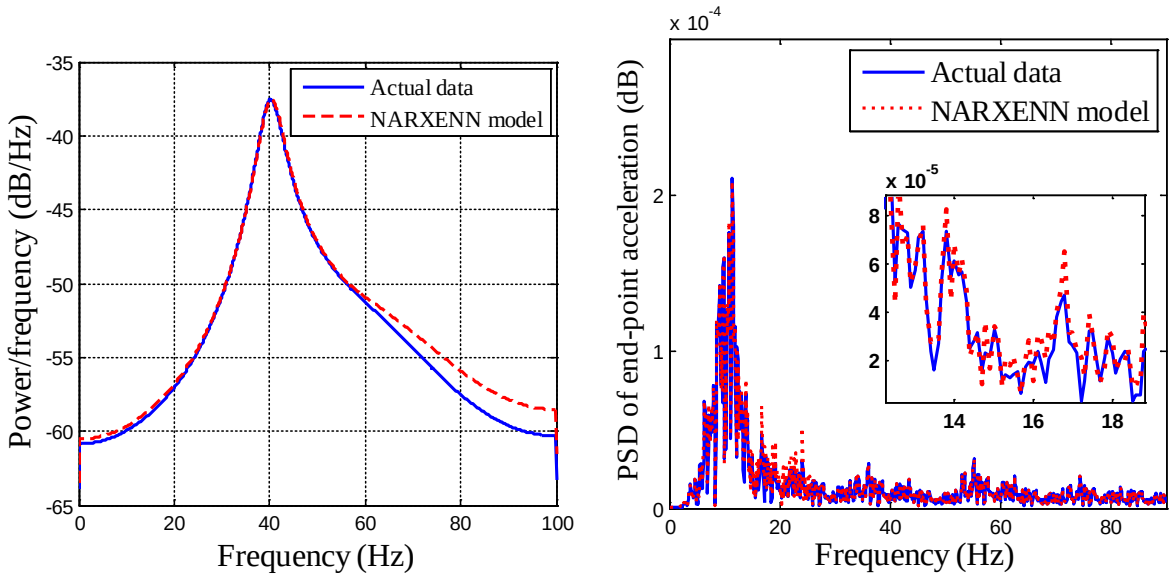

(a) **(b)**

Fig. 8. Frequency domain modeling of wiper lip response: **(a)** PSD of end-point acceleration; **(b)** Yule-Walker spectral density of end-point acceleration

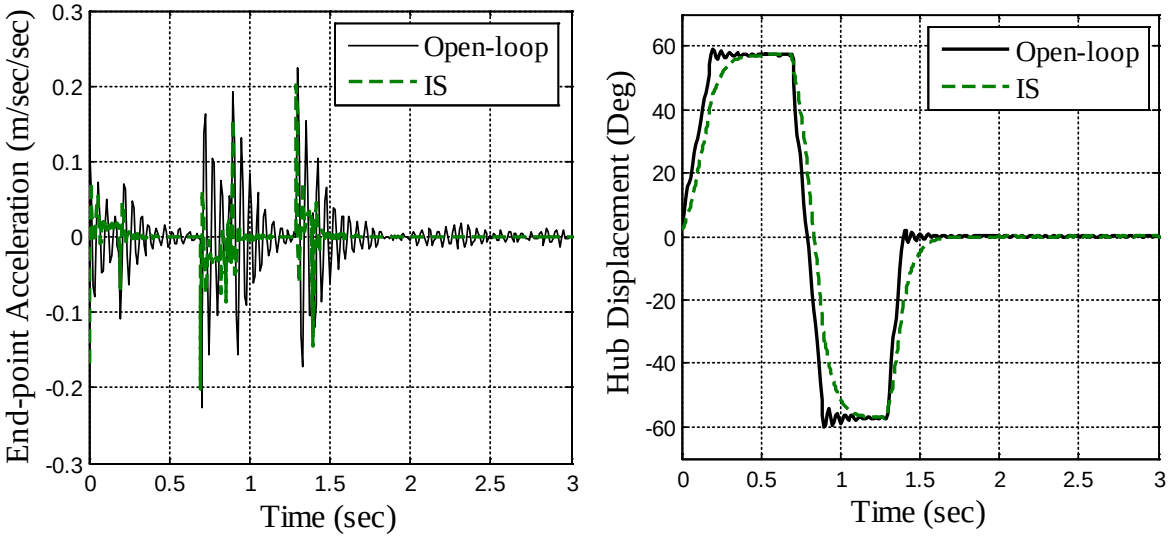

(a) **(b)**

Fig. 9. Time domain response of wiper lip without disturbance: **(a)** End-point acceleration of wiper lip; **(b)** hub displacemen

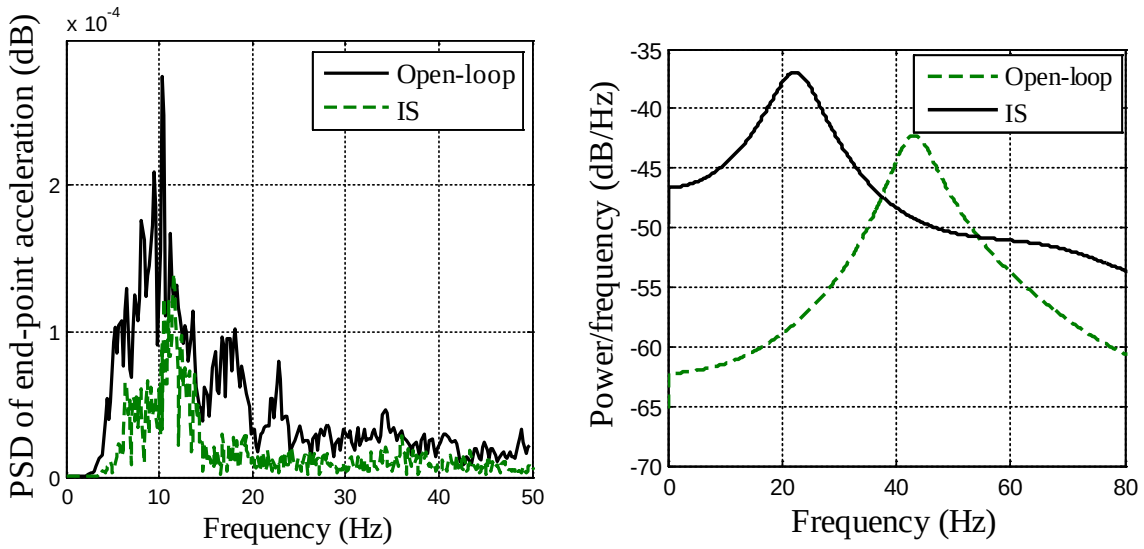

(a) **(b)**

Fig. 10. Frequency domain response of wiper lip without disturbance: **(a)** PSD of end-point acceleration; **(b)** Yule-Walker spectral density of end-point acceleration

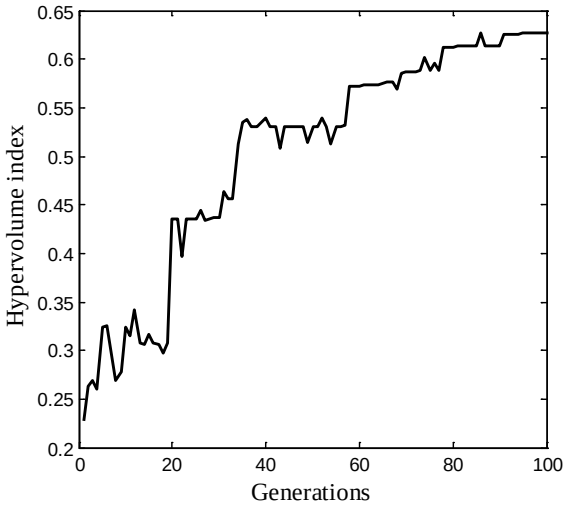

Fig. 11. Hypervolume indicator of wiper system objective space using MOGA

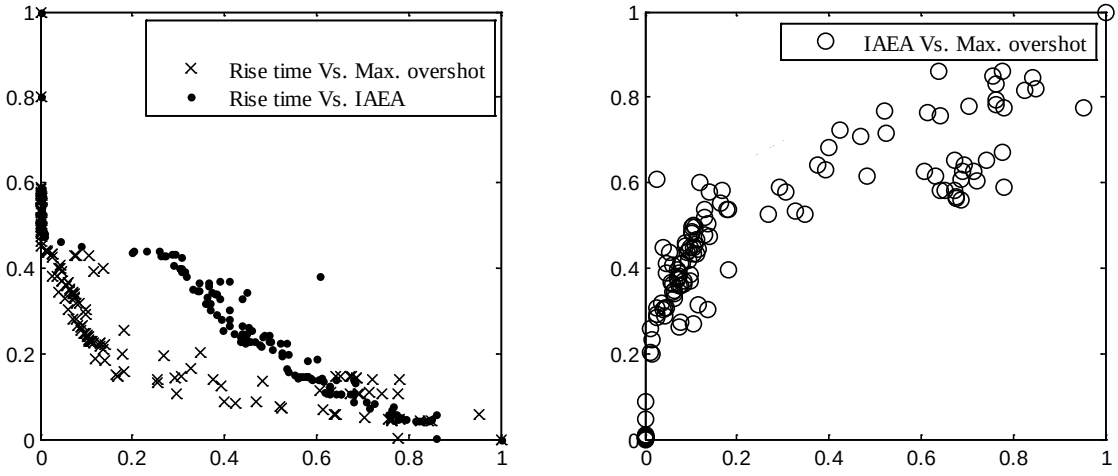

(a) **(b)**

Fig. 12. Optimal Pareto sets illustrations of pair objectives: **(a)** conflict interests; **(b)** mutual interests

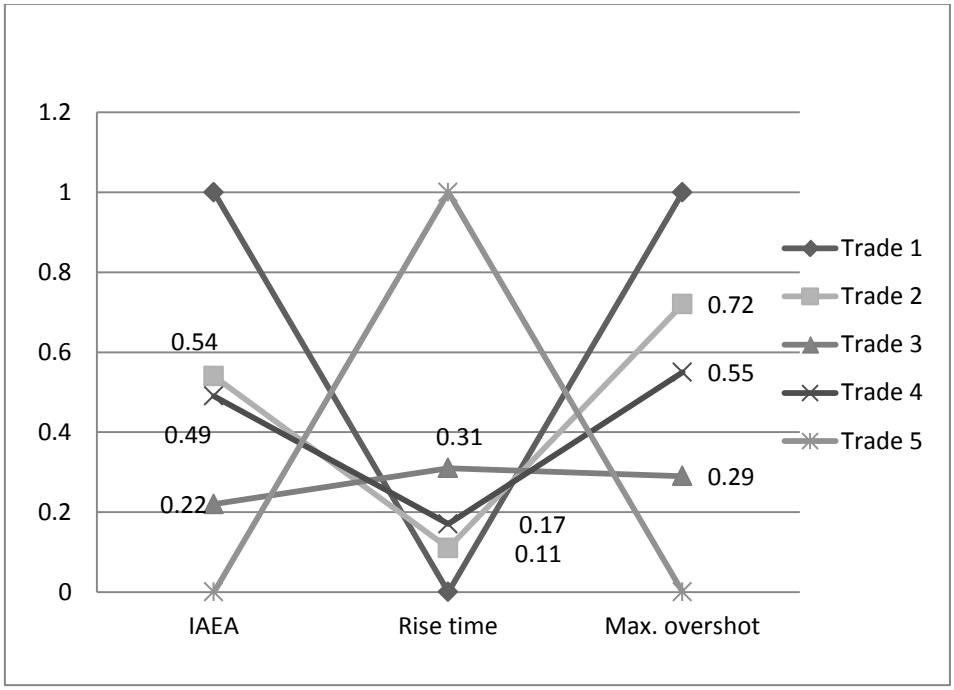

Fig. 13. Trades off samples among three objectives' Pareto set

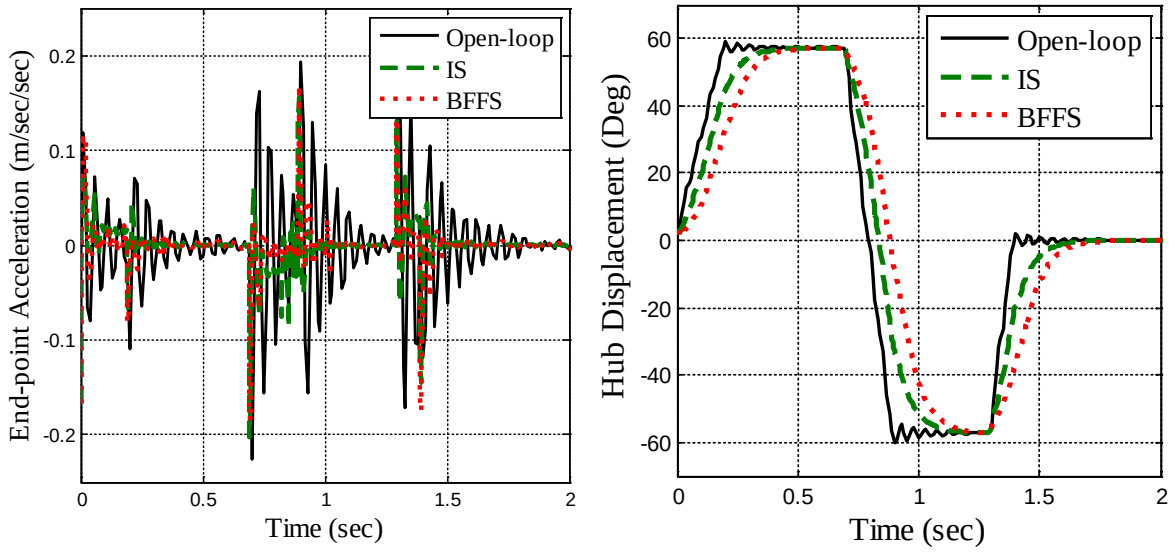

(a) **(b)**

Fig. 14. Time domain response of wiper lip in presence of disturbance: **(a)** End-point acceleration of wiper lip; **(b)** hub displacemen

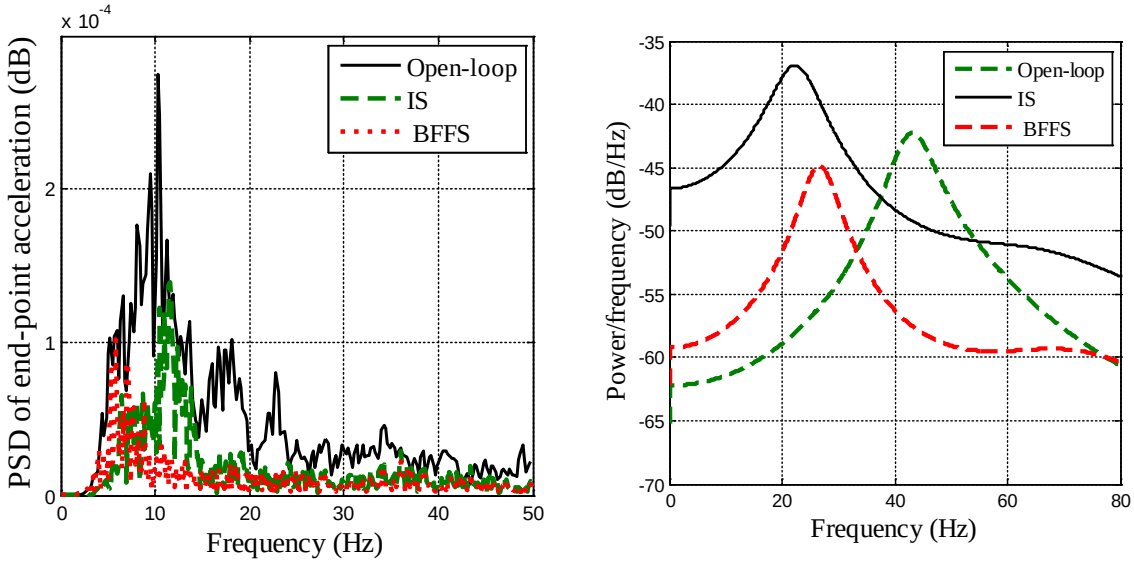

(a) **(b)**

Fig. 15. Frequency domain response of wiper lip in presence of disturbance: **(a)** PSD of end-point acceleration; **(b)** Yule-Walker spectral density of end-point acceleration

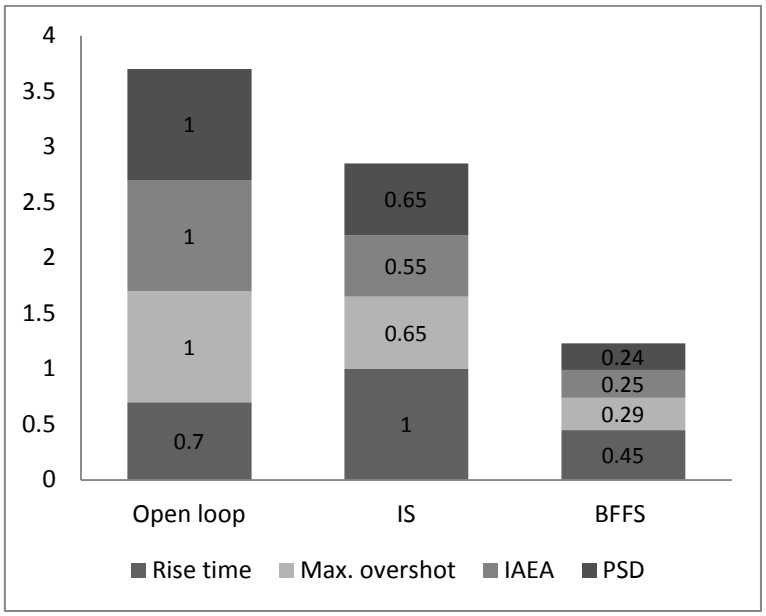

Fig. 16. Performance measurements of controllers